ELSEVIER

Colloids and Surfaces
A: Physicochemical and Engineering Aspects 206 (2002) 135–155

COLLOIDS AND SURFACES A

www.elsevier.com/locate/colsurfa

On the importance of nucleation solutions for the rupture of thin liquid films

Uwe Thiele [a,*], Kai Neuffer [a,b], Yves Pomeau [a,c,d], Manuel G. Velarde [a]

[a] *Instituto Pluridisciplinar, Universidad Complutense, Paseo Juan XXIII, 1, 28040 Madrid, Spain*
[b] *Lehrstuhl für Statistische Physik und Nichtlineare Dynamik, BTU-Cottbus, Erich-Weinert-Strasse 1, 03046 Cottbus, Germany*
[c] *Laboratoire de Physique Statistique de I'Ecole Normale Supsrieure, associè au CNRS, 24 Rue Lhomond, 75231 Paris, Cedex 05, France*
[d] *Laboratoire ASCJ, Bâtiment 506, 91405 Orsay, Cedex, France*

Abstract

The process of dewetting of a thin liquid film is usually described using a long wave approximation yielding a single evolution equation for the film thickness. This equation incorporates an additional pressure term—the disjoining pressure—accounting for the effective interaction of the thin film with the substrate. We use the equation to study the evolution of unstable thin films examining the thickness ranges for linear instability and metastability for flat films, the families of stationary periodic and localized solutions and their linear stability. From this we conclude that within the linearly unstable thickness range exists a well defined subrange where finite perturbations are crucial for the time evolution and the resulting structures. In the remainder of the linearly unstable thickness range the resulting structures are controlled by the fastest flat film mode as was assumed up to now for all the linearly unstable thickness range. The results are shown for a disjoining pressure derived by coupling hydrodynamics to the diffuse interface model and for disjoining pressures combining destabilizing [stabilizing] polar short-range interaction with stabilizing [destabilizing] apolar long-range interaction. Finally, the implications for spinodal decomposition of a binary mixture are discussed.

Keywords: Thin liquid film; Surface instability; Nucleation; Dewetting

1. Introduction

The evolution of thin liquid films on solid substrates is of huge interest in many applications like for instance coating or drying processes. Destabilizing influences leading to film rupture can arise from gradients in the surface tension caused by spatial variation of temperature or surfactant concentration fields, by evaporation or by interactions between the substrate and the film [1]. The substrate–film interactions due to molecular forces are especially important for very thin films with thicknesses smaller than hundred nanometers. The detailed understanding of the rupture process due to molecular forces that leads to dewetting is important (1) to understand how

* Corresponding author. Present address: Department of Physics, University of California, Berkeley, CA 94720-7300, USA. http://www.uwethiele.de.
E-mail address: thiele@mpipks-dresden.mpg.de (U. Thiele).

0927-7757/02/$ - see front matter
PII: S0927-7757(02)00069-9

to keep thin films stable [2] and (2) to break thin films in a controlled manner [3].

The dewetting process starts with the formation of holes in unstable films. These holes expand laterally resulting in the formation of a polygonal network of liquid rims that may break into ensembles of liquid drops [4,5]. Experimental and theoretical work investigates the initial rupture of the film [2,6–8], the growth of single holes and of the rim surrounding it [9–11], the change in time and the final state of the overall pattern [3,5,12–15] and instabilities of the liquid rim surrounding the growing hole [16–18].

Two mechanisms of film rupture are widely discussed in the literature: surface instability and heterogeneous nucleation due to defects. They occur in the range of metastable and linearly unstable film thicknesses, respectively, [2,5,7,8,12,13,19–21]. To distinguish the two mechanisms different procedures have been proposed. They are mostly based on a geometrical analysis of the final hole pattern. On the one hand, the change of the hole density averaged over the sample with film thickness is compared with the dependence of wavelength on film thickness as given by the linear stability analysis [5,22]. On the other hand, ordered and disordered arrangements of holes are taken as caused by surface instability and nucleation, respectively [12,19,21]. The analysis instruments used to determine the order of a pattern range from the pair correlation function for the set of points formed by the hole centers [21] to Minkowski measures that give higher order characteristics of the same set of points [12].

The hydrodynamic description of the dewetting process bases on the great difference between the two important lengths scales in the problem, i.e. the film thickness and the scale of lateral changes in the film profile. The disparity allows the use of the long-wave or lubrication approximation of Stokes equations [1] to derive a non-linear evolution equation for the film thickness. The formal similarity of this equation with the Cahn–Hilliard equation that describes the spinodal decomposition of a binary mixture [23] gave the name 'spinodal dewetting' to the film rupture due to the surface instability [24].

The possibly destabilizing molecular forces are included in the thickness evolution equation as an additional pressure term, the so-called disjoining pressure first introduced by Derjaguin [25,26]. Depending on the particular problem treated, the disjoining pressure may incorporate Van-der-Waals, electrostatic and structural interaction terms [27–30]. Every term of the disjoining pressure acts on its specific thickness scale and can be stabilizing or destabilizing.

A standard choice for a liquid film on a substrate is the combination of two components, normally a short- and a long-range component. Both can be destabilizing or stabilizing. Their combination gives four types of disjoining pressures [31,32] that have been used to study the two- and three-dimensional evolution of unstable films [33–36]. Including a thin coating layer on the substrate extends the number of terms and, therefore, the possible variations [8,16,37]. For all the individual terms a broad range of different functional forms, mainly exponentials or power laws are discussed in the literature (see for instance [27]). Take note, that a common shortcoming of nearly all the usually discussed disjoining pressures is its singularity for the film thickness tending to zero.

Recently, the long wave approximation for thin films was combined with a diffuse interface description for the surface of the liquid to derive a disjoining pressure that does not contain divergences for vanishing film thickness [38]. There the vertical density profile of the liquid is determined for a flat horizontal layer of fluid. Thereby they take into consideration the smooth but nevertheless relatively sharp density transition between fluid and gas, and the density variation close to the solid substrate due to molecular interactions. The latter is given by fixing the value of the fluid density at the substrate. In the case of a partially wetting situation with a small macroscopic equilibrium contact angle this value is slightly smaller than the bulk density in the liquid film. To account for dynamic situations the density profile obtained in this way is then combined with the Stokes equation in the long wave approximation. The resulting film thickness equation has the same form as the normally used thin film equation with

disjoining pressure [1]. However, in this case the disjoining pressure results from diffuse interface theory.

We use the film thickness equation with both, the disjoining pressure from diffuse interface theory [38] and a disjoining pressure combining a short-range polar and a long-range apolar component as used for instance in [31,39] to perform an analysis of the competing mechanisms leading to the rupture of a thin liquid film. By 'rupture' we mean here true rupture leading to patches of dry substrate or the formation of holes with a very thin remaining film, as in a precursor film model [40]. Which case is relevant depends, as discussed below, on the chosen disjoining pressure and interaction parameter.

Take note that our analysis in the case of the disjoining pressure from diffuse interface theory not only aims at results for film rupture on a horizontal substrate but also serves as a key study for an analyses of sliding drops on an inclined plane (see [41] in this volume).

We begin with the thin film evolution equation, discuss the disjoining pressures used and the respective scalings, introduce a Lyapunov function (free energy potential) and proceed with the derivation of the stationary equation (Section 2). Then, stability, metastability and linear instability are discussed for a flat or homogeneous film (Section 3) and different types of families of stationary inhomogeneous (periodic and localized) solutions and their linear stability are calculated (Section 4). The linear stability analysis of the periodic solutions allows to discuss their significance in the evolution process. The detailed analysis of the periodic nucleation solutions and of their linear stability leads us to the distinction of two subranges of film thickness within the linearly unstable film thickness range. For the two subranges qualitatively different behavior is predicted during structure formation. In (A), the nucleation dominated subrange, initial small-scale finite disturbances determine the final structure hence overcoming the fastest flat film mode, and in (B), the instability dominated subrange, the fastest flat film mode overcomes the finite perturbations. After having shown the importance of the nucleation solutions for the rupture process we further elaborate on their properties and the dependence of the system behavior on these properties. Up to this point all detailed calculations are done for the two disjoining pressures with destabilizing short-range and stabilizing long-range interactions thereby reviewing and extending the results of [42,43].

In Section 5 we discuss the applicability of the results for a system with a disjoining pressure combining a stabilizing short-range and a destabilizing long-range interaction. Finally, in Section 6 we compare the results for the different disjoining pressures and discuss the application of our results to the spinodal decomposition of binary mixtures [44–47].

2. The film thickness evolution equation

Using the long wave or lubrication approximation the film thickness evolution equation for a very thin liquid film on a solid substrate was derived from Stokes equation in [1]. For a two-dimensional geometry as sketched in Fig. 1 one finds:

$$\partial_t h = -\partial_x\{Q(h)\partial_x[\gamma\partial_{xx}h - \partial_h f(h)]\} \quad (1)$$

where h denotes the space- and time-dependent film thickness, and $Q(h) = h^3/3\eta$ the mobility factor due to the assumed Poiseuille flow. $\gamma\partial_{xx}h$ represents the Laplace- or curvature pressure and $\partial_h f(h)$ is an additional pressure term corresponding to the free energy $f(h)$. γ and η are the respective surface tension and viscosity of the liquid. Subscripts t, x and h denote the corresponding partial derivatives.

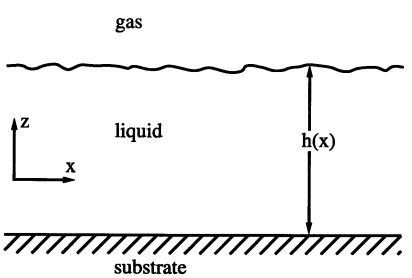

Fig. 1. Sketch of the two-dimensional geometry.

The additional pressure may comprise the different interactions between substrate and thin liquid film, i.e. the disjoining pressure, $\Pi(h)$, and/or the hydrostatic pressure. Take note, that different conventions for the sign of $\Pi(h)$ exist in the literature. Here, we use the convention $\Pi(h) = -\partial_h f(h)$, taken $\partial_h f(h)$ without the hydrostatic pressure.

In the course of the work we will investigate the following three disjoining pressures that are introduced in the next subsections:

(I) Disjoining pressure arising from diffuse interface theory and hydrostatic pressure.
(II) Destabilizing short-range polar and stabilizing long-range apolar interactions.
(III) Stabilizing short-range polar and destabilizing long-range apolar interactions.

We will use the general form $\partial_h f(h)$, in nearly all derivations and calculations and introduce the individual examples only in the final stage of calculations. In this way all derivations can be used easily whatever the particular disjoining pressure used is.

2.1. Disjoining pressure from diffuse interface theory

In case (I) the disjoining pressure from diffuse interface theory [38] is studied. Into (Eq. (1)) we introduce:

$$\partial_h f(h) = \kappa M(h, a) + \rho g h = \frac{2\kappa}{a}\,\mathrm{e}^{-h/l}\left(1 - \frac{1}{a}\,\mathrm{e}^{-h/l}\right) + \rho g h \tag{2}$$

where g is the gravitational acceleration and ρ the density of the liquid. $\Pi(h) = -\kappa M(h, a)$ is the disjoining pressure arising from diffuse interface theory, the constant κ has the dimension of a spreading coefficient per length, a is a small dimensionless positive parameter describing the wetting properties in the regime of partial wetting, l is the length scale of the diffuse interface [38] and $\rho g h$ is the hydrostatic pressure. We introduce dimensionless quantities (with tilde) using new scales:

$$t = \frac{3\eta\gamma}{\kappa^2 l}\,\tilde{t}$$

$$h = l\tilde{h}$$

$$x = \sqrt{\frac{l\gamma}{\kappa}}\,\tilde{x}. \tag{3}$$

The ratio $\kappa l/\gamma$ is $O(a^2)$ [38], i.e. the scale in x-direction is $O(l/a)$. For the film evolution Eq. (1) we find after dropping the tildes:

$$\partial_t h = -\partial_x\{h^3\partial_x[\partial_{xx}h - M(h, a) - Gh]\} \tag{4}$$

where

$$G = \frac{l\rho g}{\kappa} \tag{5}$$

stands for the ratio of gravitation and molecular interactions. Its values are taken to be always positive. It will be seen that even a very small G cannot be dropped because it is crucial for the behavior of the solutions of the system; the problem is singular at $G = 0$. The form of $M(h, a)$ allows to transfer the constant a into the mobility factor Q by introducing the shifted film thickness $h^* = h + \ln a$. After dropping the star we find:

$$M(h) = 2\mathrm{e}^{-h}(1 - \mathrm{e}^{-h}) \tag{6}$$

while the evolution Eq. (1) becomes

$$\partial_t h = -\partial_x\{Q(h)\partial_x[\partial_{xx}h - \partial_h f(h)]\} \tag{7}$$

with $Q(h) = (h - \ln a)^3$ and

$$\partial_h f(h) = M(h) + Gh \tag{8}$$

In the following we will refer to the disjoining pressure derived from diffuse interface theory as disjoining pressure (I) or case (I).

2.2. Disjoining pressure combining polar and apolar interactions

As disjoining pressure (II) we use a combination of polar short-range destabilizing and apolar (Lifshitz–Van-der-Waals) long-range stabilizing interaction that is widely used in the literature [26,31,39].

$$\partial_h f(h) = -\Pi(h) = -2S_{\mathrm{ap}}\frac{d_0^2}{h^3} - \frac{S_{\mathrm{p}}}{l}\,\mathrm{e}^{(d_0 - h)/l} \tag{9}$$

$d_0 = 0.158$ nm is the Born repulsion length and l the correlation length of a polar fluid [31]. $S_{\mathrm{p}} < 0$ and $S_{\mathrm{ap}} > 0$ are the polar and apolar components

of the total spreading coefficient, $S = S_{ap} + S_p$. Experimental systems corresponding to this case are for instance water on graphite [21] and on most polar substrates like PMMA, corneal epithelium, PVC or polystyrene [31,39]. Introducing the dimensionless parameters.

$$\kappa = \frac{|S_p|}{l}\, e^{d_0/l} \text{ and } b = \frac{2|S_{ap}|d_0^2}{|S_p|l^2}\, e^{-d_0/l} \tag{10}$$

and using the same scaling, Eq. (3), as in case (I) one obtains again the dimensionless film evolution Eq. (7) but this time with the mobility factor $Q(h) = h^3$. The dimensionless free energy is:

$$f(h) = \frac{b}{2h^2} - e^{-h} \tag{11}$$

We will refer to this case as disjoining pressure (II). Another interesting situation, denoted here case (III), is the inverse of case (II), namely, the combination of a stabilizing polar short-range ($S_p > 0$) and a destabilizing apolar (Lifshitz–Vander-Waals) long-range interaction ($S_{ap} < 0$). This corresponds for instance to DMSO on talc, HSA or ephitelium [31,33,39].

In our notation the disjoining pressure for this case is also given by Eq. (9) but with $S_p > 0$ and $S_{ap} < 0$. Using the same scales as in cases (I) and (II), Eq. (3), the film thickness equation is again Eq. (7). However, the free energy is now:

$$f(h) = -\frac{b}{2h^2} + e^{-h} \tag{12}$$

This case, referred to as disjoining pressure (III), will be discussed in Section 5.

2.3. Lyapunov functional

At different points of our work we need a valid energy measure that can be assigned to a given film thickness profile, $h(x, t)$. Following for instance [24,46,48], we introduce the semidefinite positive functional:

$$F(h) = \int \left[\frac{1}{2}(\partial_x h)^2 + f(h) - C_1(h - \bar{h})\right] dx \tag{13}$$

which we shall show is a Lyapunov functional, $\bar{h}$ stands for the mean film thickness and C_1 is the Lagrange multiplier for material conservation that is needed to compare different stationary solutions with identical volume of liquid. To show that $F(h)$ is a Lyapunov functional we have to show that its functional derivative is semidefinite negative. The evolution equation Eq. (7) is written as:

$$\partial_t h = \partial_x \left(Q(h) \partial_x \frac{\delta F}{\delta h} \right) \tag{14}$$

with δ denoting functional variation. Multiplying Eq. (14) by $\delta F/\delta h$ and integrating with respect to x gives, after integration by parts, the total time derivative of F:

$$\frac{dF}{dt} = -\int Q(h) \left(\partial_x \frac{\delta F}{\delta h} \right)^2 dx. \tag{15}$$

For positive film thicknesses the mobility factor, $Q(h)$, is always positive implying that the derivative dF/dt is always negative, i.e. F is a valid Lyapunov or energy functional. We will call it shortly 'energy'. It can be used to compare stationary solutions to determine their absolute stability and measure their time evolution in the numerical integration of Eq. (7).

2.4. Stationary equation

To study stationary and especially homogeneous or flat film solutions we set the time derivative, $\partial_t h$, to zero and integrate Eq. (7), yielding:

$$0 = Q(h)[\partial_{xxx} h - (\partial_{hh} f(h))\partial_x h] + C_0 \tag{16}$$

We are looking for three types of solutions bounded in h: (a) flat film solutions (b) localized solutions, and (c) periodic solutions. For (a) and (b) the integration constant C_0 can be set to zero because all x-derivatives vanish for x tending to infinity. For (c) the reflection symmetry with respect to the extrema of the solutions also implies $C_0 = 0$. In consequence one can integrate a second time to obtain:

$$0 = \partial_{xx} h(x) - \partial_h f(h) + C_1 \tag{17}$$

Take note that this equation can also be derived through minimization of the energy functional (Eq. (13)). The integration constant $C_1 \neq 0$ is determined by external conditions like chemical potential, vapor pressure or mass conservation.

Regarding here only the latter, the choice $C_1 = \partial_h f(h_0)$ ensures a flat film solution of Eq. (17), namely $h(x) = h_0$. Searching for localized solutions, the same $C_1(h_0)$ implies h_0 as the film thickness for $x \to \infty$. For periodic solutions, h_0 is the thickness at the inflection point of the respective profile where the curvature $\partial_{xx}h(x)$ is equal to zero. In this case the difference between h_0 and the maximal [minimal] thickness of one period is a measure of the curvature at the maximum [minimum].

Before studying periodic solutions of Eq. (17) below in Section 4 we discuss in the next section the flat film solutions of Eq. (17) and their linear and absolute stability.

3. Flat film solutions

Choosing a h_0 gives by construction the thickness of a flat film solution or fixed point of Eq. (17). Due to the nonlinear dependence of C_1 on h_0, giving the constant C_1 by the choice of h_0, allows also for other flat film solutions $h(x) = h_f$. These are determined by:

$$\partial_h f(h_f) = \partial_h f(h_0) = C_1 \tag{18}$$

For disjoining pressure (I) they are given by the crossing points of the curve $M(h) - M(h_0)$ with the straight line $-G(h - h_0)$ (see Figure 2 in [43]). For $G > 0$ one finds one or three fixed points depending on the value of G and h_0. The same crossover is observed for disjoining pressures (II) and (III) when changing b and h_0. The bifurcation points between the two regimes are characterized by $\partial_{hh}f(h_0) = 0$ and Eq. (18). For all disjoining pressures discussed we find a critical point characterized by Eq. (18) and $\partial_{hh}f(h_c) = \partial_{hhh}f(h_c) = 0$. It is situated for case (I) at ($G_c = 1/4$, $h_c = \ln 4$) and for case (II) and (III) at ($b_c = 256/3e^4 \approx 1.56$, $h_c = 4$). For $G > 1/4$ and $b_c > 256/3e^4$, respectively, there exists independently of the value of h_0 only the fixed point h_0. Take note, that close to the critical point Eq. (7) reduces to the Cahn–Hilliard equation describing the decomposition process of a binary mixture [23] (shown in [43]). By linearizing Eq. (17) close to the fixed points one finds that for $\partial_{hh}f(h_f) > 0$ they are saddles and for $\partial_{hh}f(h_f) < 0$ they are centers corresponding to the results of the linear stability analysis for flat films shown next. Bifurcation diagrams for flat film solutions for disjoining pressure (I) for fixed h_0 and fixed G, respectively, are shown in [43].

3.1. Linear stability of flat film solutions

To determine the linear stability of the flat film solutions we use a Fourier mode decomposition of the perturbation:

$$h(x) = h_0 + \varepsilon e^{\beta t + ikx}. \tag{19}$$

$\varepsilon \ll 1$ is the amplitude of the mode and β and k are, respectively, the growth rate and wave number of the disturbance. Linearizing the full time dependent Eq. (7) in ε using the ansatz (Eq. (19)) yields:

$$\beta = -Q(h_0)k^2[k^2 + \partial_{hh} f(h_0)] \tag{20}$$

The film is linearly unstable for positive growth rates, β, i.e. for $k = 0$ it is unstable for:

$$\partial_{hh} f(h_0) < 0 \tag{21}$$

Accordingly, for cases (I) and (II) there is a range of linearly unstable thicknesses at intermediate values:

$$h_i^d < h_0 < h_i^u \tag{22}$$

whereas, for case (III) flat films are always linearly unstable outside a thickness range at intermediate values that is identical to the linearly unstable thickness range in case (II). For case (I) the limiting thickness values are given by:

$$h_i^{u/d} = -\ln\left[\frac{1}{2}\left(\frac{1}{2} \mp \sqrt{\frac{1}{4} - G}\right)\right] \tag{23}$$

For $G \ll 1$ one has $h_i^d \approx -\ln(G/2)$ and $h_i^u \approx \ln 2 + G$. In the limit $G \to 0$ there is no upper limit for the instability range as even very thick films are unstable, and hence we cannot set G to zero without changing the qualitative behavior of the system. As shown in [43] close to the critical point ($G_c = 1/4$, $h_c = \ln 4$), Eq. (23) simplifies to $h_i^{u/d} = h_c \pm 2\sqrt{G_c - G} + O(G_c - G)$. The linearly unstable thickness range lies to the left of the solid line in Fig. 2(a).

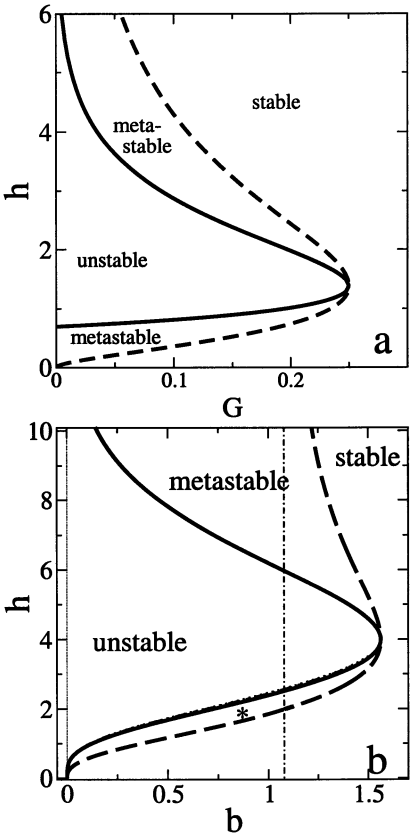

Fig. 2. Stable, linearly unstable and metastable film thickness ranges for disjoining pressures (a) from diffuse interface theory (I) and (b) combining destabilizing short-range polar and stabilizing long-range apolar interaction (II). The dot-dashed line in (b) gives the value $b = 8/e^2$. For smaller b there exists no upper stable film thickness range. The star denotes the lower metastable range.

In cases (II) and (III) no analytical expression as Eq. (23) can be given, the border of the linearly unstable region has to be calculated numerically. For $b \to 0$ no upper limiting value exists and the lower limit scales as $h_i^d = (3b)^{1/4}$. Close to the critical point ($b_c = 256/3e^4$, $h_c = 4$), one finds as in case (I) $h_i^{u/d} = h_c \pm 2\sqrt{b_c - b} + O(b_c - b)$. The linearly unstable thickness range for case (II) [(III)] lies to the left [right] of the solid line in Fig. 2(b). For case (III) see also below Fig. 13. For all disjoining pressures the critical (smallest unstable) wavelength for a given film thickness, h_0, as given by the condition $\beta = 0$, is:

$$\lambda_c = \frac{2\pi}{\sqrt{-\partial_{hh} f(h_0)}} \tag{24}$$

This implies that the thickness profile $h(x) = h_0 + \varepsilon \exp(ik_c(h_0)x)$ with $k_c(h_0) = 2\pi/\lambda_c = \sqrt{-\partial_{hh} f(h_0)}$ is neutrally stable and represents a infinitesimally small amplitude stationary solution of Eq. (17).

The fastest growing linearly unstable mode has the wavelength $\lambda_m = \sqrt{2}\lambda_c$ and the growth rate:

$$\beta_m = \frac{1}{4} Q(h_0)[\partial_{hh} f(h_0)]^2 \tag{25}$$

The linear stability results are indeed related to the type of fixed points discussed in Section 3: linearly unstable [stable] flat films correspond to center [saddle] fixed points.

3.2. Absolute stability of flat film solutions

It is possible that a linearly stable flat film may be unstable to finite amplitude disturbances. This corresponds to a metastable flat film. Only if, for a given film thickness there is no stationary thickness profile with smaller energy the flat film is absolutely stable. To study this issue the existence of a flat film of thickness h_0 extended from $-\infty$ to ∞ is assumed. Then, a small part of finite length s is given the thickness h, ensuring that the mean film thickness remains h_0. Also, one assumes that the width of the transition region between the two thickness levels is small compared with the length s, so the gradient part, $(\partial_x h)^2$, of the energy Eq. (13) can be neglected. Now the energy per unit length of the changed part, g, is calculated using the Lyapunov functional (Eq. (13)):

$$g(h) = f(h) - C_1(h_0)h + C_1(h_0)h_0 \tag{26}$$

Dropping the constant part $C_1(h_0)h_0$ the function $g(h) - C_1(h_0)h_0$ has different number of maxima and minima depending on the disjoining pressure used and the mean film thickness, h_0. For disjoining pressure (II), $g(h) - C_1(h_0)h_0$ is plotted in Fig. 3 for different values of the mean film thickness, h_0, and two different b. Disjoining pressure (I) gives for all G qualitatively similar curves as Fig. 3(b), whereas for disjoining pressure (III) Fig. 3 is valid taking $g \to -g$.

In a situation described qualitatively by Fig. 3(b) the two minima of $g(h)$ represent the lower and upper linearly stable thicknesses discussed in Section 3.1. However, only the deeper minimum corresponds to an absolutely stable film thickness, whereas the other one is a metastable state. The maximum represents the linearly unstable thicknesses as in Section 3.1. The metastable thickness range is limited by the value of h_0 where the two minima in Fig. 3(b) have the same depth. There exist an upper and a lower limit, that we denote $h_{\mathrm{m}}^{\mathrm{u}}$ and $h_{\mathrm{m}}^{\mathrm{d}}$, respectively. They are characterized by:

$$\partial_h f|_{h_{\mathrm{m}}^{\mathrm{u}}} = \partial_h f|_{h_{\mathrm{m}}^{\mathrm{d}}} \tag{27}$$

and

$$g(h_{\mathrm{m}}^{\mathrm{u}}) = g(h_{\mathrm{m}}^{\mathrm{d}})$$

Note, that the solutions of Eq. (27) correspond also to the conditions determining the two equilibrium film thicknesses that are reached by a thin film system at the end of the time evolution as obtained in [24,18,49] by a Maxwell construction.

In case (I) these two thicknesses can be found analytically for small enough, but not vanishing $G \ll 1$, using the assumptions $h_{\mathrm{m}}^{\mathrm{u}} \gg 1$ and $h_{\mathrm{m}}^{\mathrm{d}} \ll 1$. To lowest order in G, Eq. (27) yield $h_{\mathrm{m}}^{\mathrm{d}} = \sqrt{G/2} + O(G)$ and $h_{\mathrm{m}}^{\mathrm{u}} = \sqrt{2/G} + O(G^{1/2})$. Analytical approximations can also be found close to the critical point ($G_{\mathrm{c}} = 1/4$, $h_{\mathrm{c}} = \ln 4$). To lowest order we have $h_{\mathrm{m}}^{\mathrm{u/d}} = h_{\mathrm{c}} \pm 2\sqrt{3(G - G_{\mathrm{c}})} + O(G - G_{\mathrm{c}})$ as derived in [43]. Linearly unstable, metastable and stable thickness ranges are shown in Fig. 2(a).

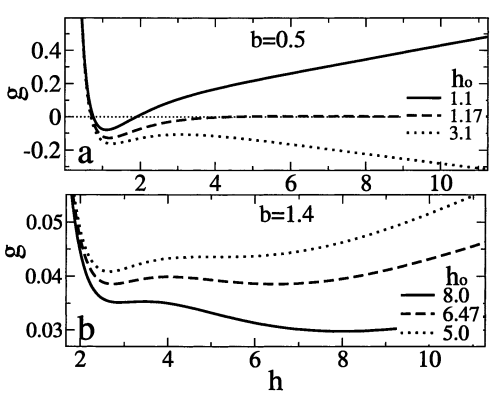

Fig. 3. The energy, g, for disjoining pressure (II) for (a) $b = 0.5$ and (b) $b = 1.4$. Shown are curves for different film thicknesses h_0, as given in the legends.

In case (II) the function $g(h)$ has the two qualitatively different forms of a single-well potential as in Fig. 3(a) and a double-well potential as in Fig. 3(b) for $b < 8/\mathrm{e}^2$ and $b_c > b > 8/\mathrm{e}^2 = 1.08$, respectively. For every b the metastable thickness range is limited by the h_0 allowing for two minima of equal depth. For $b > 8/\mathrm{e}^2$ there exist upper and lower limits as discussed above in case (I), whereas for $b < 8/\mathrm{e}^2$ no upper limit of the metastable range exists and the lower limit is given by $\partial_h f\,|h_{\mathrm{m}}^{\mathrm{d}} = 0$, securing $g(h \to \infty) = 0$. For $b \to 0$ the lower limit approaches zero as $h_{\mathrm{m}}^{\mathrm{d}} = b^{1/3}$. Linearly unstable and metastable thickness ranges are shown in Fig. 2(b).

In case (III) function $g(h)$ can have one local minimum at intermediate film thicknesses. However, this can never be the global minimum because $g(h) \to -\infty$ for small h (inverse of Fig. 3(a)) or for both, small and large h (inverse of Fig. 3(b)). In consequence, every film thickness in the linearly stable range is only metastable as indicated below in Fig. 13.

The results for linear stability and metastability of flat films are valid for two- and three-dimensional film geometries. However, from now on we restrict our attention to the two-dimensional geometry, i.e. to film profiles depending on only one spatial co-ordinate, x.

4. Periodic and localized solutions

To study periodic solutions of Eq. (17), it is multiplied by h_x and integrated:

$$\partial_x h = \sqrt{2}\sqrt{f(h) - (\partial_h f(h_0))h - C_2}. \tag{28}$$

One chooses

$$C_2 = f(h_{\mathrm{m}}) - (\partial_h f(h_0))h_{\mathrm{m}} \tag{29}$$

where for periodic solutions h_{m} is the minimal or maximal thickness, whereas for localized solutions $h_{\mathrm{m}} = h_0 = h_\infty$. Every solution can be parameterized by the pair (h_0, h_{m}) or (C_1, C_2). Eq. (29) allows to plot the solutions in the phase plane (h, h_x). In the parameter range with only one fixed point there exist no bounded solutions beside the

imposed flat film solution $h(x) = h_0$. In the parameter range allowing for three fixed points, one obtains three qualitatively different phase portraits as shown in [24,43]. Depending on the parameters G or b and h_0 one encounters (a) the drop, (b) the front and (c) the hole regime. In the hole [drop] regime one finds beside periodic solutions an homoclinic solution connecting the highest [lowest] fixed point with itself. This represents a localized hole [drop] in an otherwise flat film and can be seen as the limiting case of a periodic solution with infinite period. Holes [drops] can be found in a continuous range of the parameter plane that corresponds exactly to the upper [lower] metastable range for flat films discussed above. Take note, that not for all cases discussed here exist both ranges.

In the front regime one finds periodic solutions and an heteroclinic solution connecting the lowest and the highest fixed point. The latter represents a localized front solution that connects two semi-infinitely extended flat films of thicknesses, $h_{\mathrm{m}}^{\mathrm{d}}$ and $h_{\mathrm{m}}^{\mathrm{u}}$. The front exists only for a single line in the parameter plane, identical to the border between metastable and stable flat films as given by Eq. (27). Consequently, no front solutions exist in case (III) and in case (II) for $b < 8/\mathrm{e}^2$.

The existence of periodic solutions was already discussed for qualitatively similar disjoining pressures [24,30]. In [50,51] similar hole and drop solutions were found close to a first order wetting transition and identified as critical nuclei. Our study of the energy of the solutions supports this finding also in our case. From now on we concentrate on the periodic solutions, but remember that the localized solutions are also a limiting case of periodic solutions.

To discuss the importance of the periodic solutions in the time evolution of unstable non-evaporating liquid films we determine the existing families of periodic solutions for a given mean film thickness, $\bar{h}$. The solutions are characterized by their period, amplitude, energy and linear stability. To numerically calculate the periodic solutions of Eq. (17) we start from the analytically known, small amplitude solutions discussed in Section 3.1 for some given $\bar{h}$ in the linearly unstable film thickness range. Using a continuation procedure in the parameter space [52] the families of finite amplitude solutions are then calculated. Continuation can for instance follow a family of solutions fixing the mean film thickness and changing the period, but it is also possible to fix the period and change the mean film thickness in order to get a starting solution in the metastable film thickness range where no small amplitude solutions exist. Beside continuation, close to the border between linearly stable and unstable flat films and close to the critical point we use analytical solutions derived in [43].

To determine the linear stability of the periodic solutions obtained in this way one linearizes the full time dependent Eq. (7) using the ansatz

$$h(x) = h_0(x) + \varepsilon h_1(x) e^{\beta t} \tag{30}$$

for the disturbed solution. $h_0(x)$ is the stationary periodic solution. Introducing Eq. (30) in Eq. (7) gives to $O(\varepsilon)$:

$$\begin{aligned}\beta h_1 = {} & \{[3q^2(h_{0x} f_{hh} - h_{0xxx})]_x + (q^3 h_{0x} f_{hhh})_x\} h_1 \\ & + [2q^3 h_{0x} f_{hhh} + 3q^2(2h_{0x} f_{hh} - h_{0xxx})] h_{1x} \\ & + q^3 f_{hh} h_{1xx} - 3q^2 h_{0x} h_{1xxx} - q^3 h_{1xxxx}\end{aligned} \tag{31}$$

where $q = Q(h_0(x))^{\frac{1}{3}}$ and all derivatives of f are functions of the periodic solution $h_0(x)$. For a disturbed flat film Eq. (31) reduces to Eq. (20). Eq. (31) is, after discretizing, numerically solved as an algebraic eigenvalue problem:

$$\beta h_1 + L(h_0, h_{0x}, h_{0xx}, h_{0xxx}, h_{0xxxx}, f_h, f_{hh}, f_{hhh}) h_1 = 0 \tag{32}$$

where L is a linear operator determined by the periodic solution, h_0. The largest eigenvalues give the growth rates, β, and the corresponding eigenvectors, h_1, give the shape of the most dangerous disturbances.

Here, we introduce the different types of families using the disjoining pressure (II) as example and illustration. However, nearly all results are also qualitatively valid for disjoining pressure (I) as shown in detail in [43]. The qualitatively different case (III) is discussed after establishing all the main concepts below in Section 5.

Within the range of mean film thicknesses that correspond to linearly unstable or metastable flat films, for all $0 < b < b_{\mathrm{c}}$ we find three qualitatively

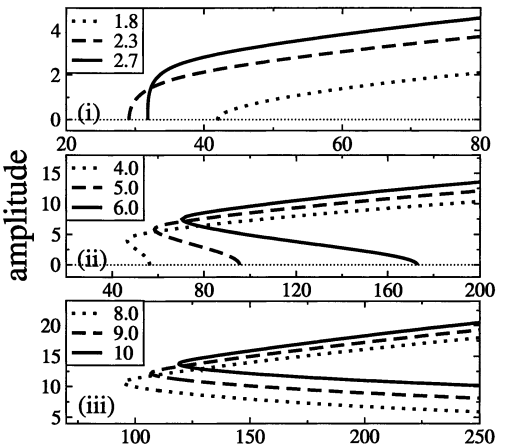

Fig. 4. Dependence of solution amplitude on period for disjoining pressure (II) at fixed $b = 0.5$. The respective mean film thicknesses, $\bar{h}$, are shown in the insets. (i) and (ii) denote the regimes within the linearly unstable film thickness range where solution families without nucleation branch and with nucleation branch are found, respectively. (iii) shows solution families in the metastable film thickness range.

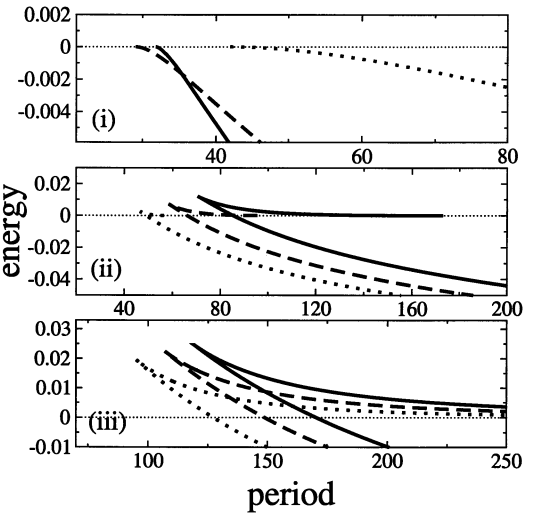

Fig. 5. Shown is the energy-period dependence for the solution families shown in Fig. 4. The energies are given relative to the respective flat film energies. (i), (ii), (iii) and the line styles are as in Fig. 4.

different families of solutions depending on mean film thickness. The definition of these families is based on the dependence of the solution amplitude on period (shown for fixed b in Fig. 4), the dependence of the energy of the solution on period (Fig. 5) and the dependence of the linear growth rate of the fastest growing disturbance on period (Fig. 6) For the purpose of illustration we choose film thicknesses ranging from within the linearly unstable range to the upper metastable range. The same sequence of behavior is found going towards the lower metastable range. However, there the film thickness region for family type (ii) is very small. We distinguish three regions with corresponding family types.

(i) The corresponding flat film is linearly unstable. There exists only one branch of stationary solutions. Amplitude increases (Fig. 4(i)) and energy decreases (Fig. 5(i)) monotonically with increasing period. The energy of the periodic solutions is always lower than the energy of the corresponding flat film. The solutions are linearly stable if one takes one period as the unit for the stability analysis (Fig. 6(i)).

(ii) The corresponding flat film is linearly unstable as in (i), but. there exist two branches of stationary solutions. The branch with the higher energy ends at a finite period (Fig. 5(ii)) with the amplitude going to zero (Fig.

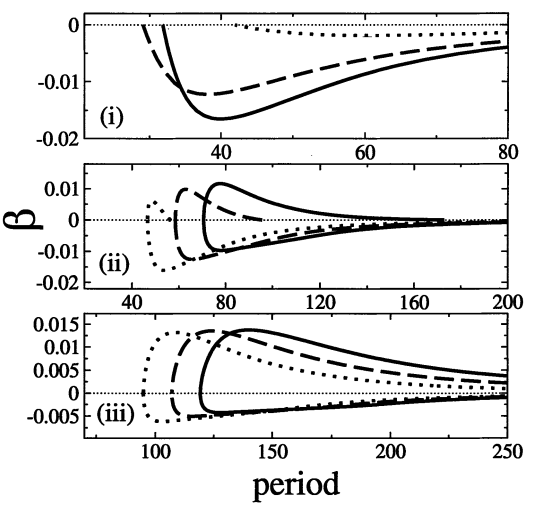

Fig. 6. Shown is the dependence of the growth rate of the fastest perturbation to the stationary periodic solutions characterized in Figs. 4 and 5 on their period. (i), (ii), (iii) and the line styles are as in Fig. 4.

4(ii)). The period where the branch terminates corresponds to the wavelength λ_c of the neutrally stable solution obtained in the linear analysis (Eq. (24)). The energy of the terminating branch is always higher than the corresponding energy of the flat film. This branch represents the nucleation solutions that have to be 'overcome' if the film is to break into finite portions with size $p < \lambda_c$. This is shown also by the linear instability of this branch (Fig. 6(ii)) and was checked by integration in time of Eq. (7) for different initial finite sinusoidal disturbances. They shrink if their amplitude is smaller then the amplitude of the corresponding nucleation solution and they grow if it is larger. The properties of the low energy branch correspond to the properties of the single branch in (i). However, although the energy of the lower branch decreases very rapidly with increasing period there is a very small period range where the energy of the flat film is smaller than the energy of both periodic solutions. This implies the absolute stability of flat films in systems of this size. Consequently, for this range of periods the low-energy periodic solution is only metastable.

(iii) The corresponding flat film is metastable. There exist two branches of periodic solutions that both continue towards infinite period. The upper branch in the period-energy plot (Fig. 5(iii)) represents again linearly unstable nucleation solutions of different periods that separate energetically the lower periodic solution from the linearly stable flat film solution (Fig. 6(iii)). Corresponding to this branch is the small amplitude branch in (Fig. 4(iii)). The single critical nucleus—the 'true' nucleation solution—is the solution that one finds following this branch towards infinite period. This is the critical drop/hole discussed for the wetting transition in [50,51]. The branch with lower energy corresponds again to the branch known from (i). As in (ii), depending on the system size, the flat film and the small-energy periodic solutions are absolutely stable and metastable, or metastable and absolutely stable, respectively.

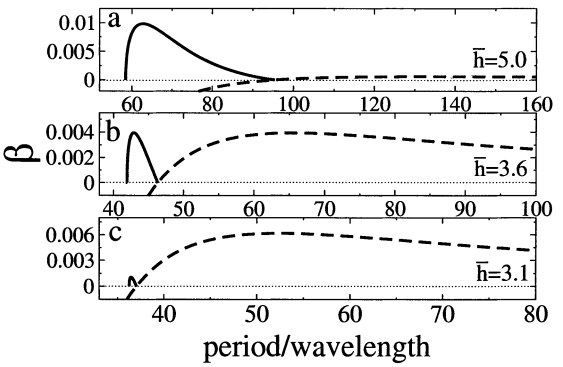

Fig. 7. Dependence of the linear growth rate of disturbances, β, on the period for nucleation solutions (solid lines) and on the wavelength for flat film solutions (dashed lines) at different values of $\bar{h}$ for disjoining pressure (11) with $b = 0.5$.

These results illustrated here in Figs. 4–6 for disjoining pressure (II) are also valid for disjoining pressure (I) [43] and, as is shown below in Section 5, with some modifications also for case (III). We expect similar results for all types of disjoining pressures used in the literature. The analysis of the families of stationary solutions of Eq. (1) implies that the distinction between instability range and nucleation range of the film thickness that is generally used in the literature should be modified towards the three ranges: (i) instability range, (ii) range of mixed behavior, and (iii) nucleation range that are shown for disjoining pressures (I), (II) and (III) in Figs. 8, 9 and 13, respectively.

One may argue, that the study of solution families and their energy tells something about equilibrium constellations under certain conditions, but does not reveal what will actually happen in the physical system during the rupture process within the thickness range with mixed behavior. To clarify this issue, we discuss first in detail the linear stability of the periodic nucleation solutions in range (ii), and second the results of a direct integration in time performed in [42]. For a given $\bar{h}$ we calculate the linear growth rates of disturbances to the solutions of the branch of nucleation solutions in the mixed range, (ii). Again we take one period of the respective solutions as the unit of the stability analysis. Fig. 7 shows the comparison of the obtained linear

growth rates and the linear growth rates for the flat film modes for the same mean film thickness, $\bar{h}$, obtained with Eq. (20). We note, that the growth rate for the nucleation solution depends non-monotonically on its period. Its maximal value can be much larger or much smaller than the maximal value of the growth rate of the linear modes for the corresponding flat film. Taking this result in its exact mathematical sense one can only state, that for linearly unstable flat films there exists a thickness range—the nucleation-dominated range—where some periodic finite perturbations corresponding to certain nucleation solutions yield linear growth rates much larger than the linear growth rate of the fastest flat film mode. However, taking this result as a hint on the local structure of the flow, $\partial_t h$, close to these nucleation solutions, we assume that in the nucleation-dominated range, local finite perturbations of a lateral extension smaller than the critical wavelength for flat film modes, λ_c, have a crucial influence on the structure formation, whereas they have negligible role in the instability-dominated range. This was shown by directly integrating the time depending Eq. (7) for disjoining pressures (I) in [43] and for disjoining pressure (II) in [42] taking as an initial condition a flat film with a localized disturbance. Here, we describe these results only verbally, but show in Section 5 detailed results for disjoining pressure (III), where the same difference is found (Figs. 20–22). The results of the time evolution for many different initial disturbances and mean thicknesses showed the qualitative distinction of the two thickness ranges within the linearly unstable thickness range.

4.1. Nucleation-dominated region (A)

The initial disturbance grows downwards forming a hole with rims at its two sides. This hole then expands laterally. Eventually, the thickness depressions at the outer bases of the rims lead to secondary nucleation events. The final, short-time structure (before coarsening sets in) is a set of holes with distances unrelated to the wavelength of the fastest growing flat film mode. The details of the process and of the resulting structure depend strongly on the width and depth of the initial disturbance. In the evolution of the energy one can clearly distinguish the individual secondary nucleation events, giving the process a step-like character. The secondary nucleation becomes less important for mean film thicknesses closer to the border of the linearly unstable range.

4.2. Instability-dominated region (B)

The initial disturbance starts to grow downwards as in (A) but from the beginning undulations on its both sides also grow rapidly. The undulations have the wavelength of the most unstable flat film mode and extend laterally with approximately constant velocity. The final short-time structure is a periodic set of holes nearly independent of the width and depth of the initial perturbation. The energy decreases approximately linear with time indicating that the lateral extension of the undulation is a smooth process with approximately constant velocity. In contrast to (A) different initial disturbances lead to the same energy for the final short-time structure. This energy is equal to the energy of the stationary solution of the period that corresponds to the wavelength of the fastest flat film mode, λ_m.

The difference found in the time evolution confirmed the above introduced separation in two experimentally distinguishable subranges—the nucleation-dominated (A) and the instability-dominated (B)—within the linearly unstable range. We delineate a border between the two subranges using the results of the linear stability analysis shown in Fig. 7. The border is defined to be at the film thickness where the maximum growth rates of the flat film mode, given by Eq. (25), and that of the periodic nucleation solution are equal as in Fig. 7(b). The numerically calculated values are plotted for disjoining pressure (I) in Fig. 8(a and b), for $h > h_c$ and $h < h_c$, respectively. For disjoining pressure (II) and (III) they are shown in Fig. 9 and Fig. 13, respectively. However, for a detailed explanation of Fig. 13 see Section 5.

Numerical integration of Eq. (7) showed that a bit away from the here defined transition line between the subranges (A) and (B) the size of the

initial disturbance has no influence on *which* of the two scenario occurs, but only on *how* it occurs (in subrange (A)). However, in the transition region close to the border defined with the help of the linear stability analysis the size of the initial disturbance also influences *which* process occurs due to the fact that in situations close to equal fastest linear growth rates for flat film modes and periodic nucleation solutions as in Fig. 7(b) only part of the periodic solutions may grow faster than the fastest flat film mode. Therefore, between (A) and (B), depending on depth and width of the initial disturbance one finds behavior corresponding to (A) or (B) or combinations of both. In the latter case the details depend also on system size. To further characterize the nucleation solutions and better estimate their influence in the transition region we show in Fig. 10 for disjoining pressure (I) the wave number ranges for linearly unstable flat film modes and periodic nucleation solutions depending on the mean film thickness, $\bar{h}$. We defined a wave number for the periodic solutions in analogy to the wave number for harmonic

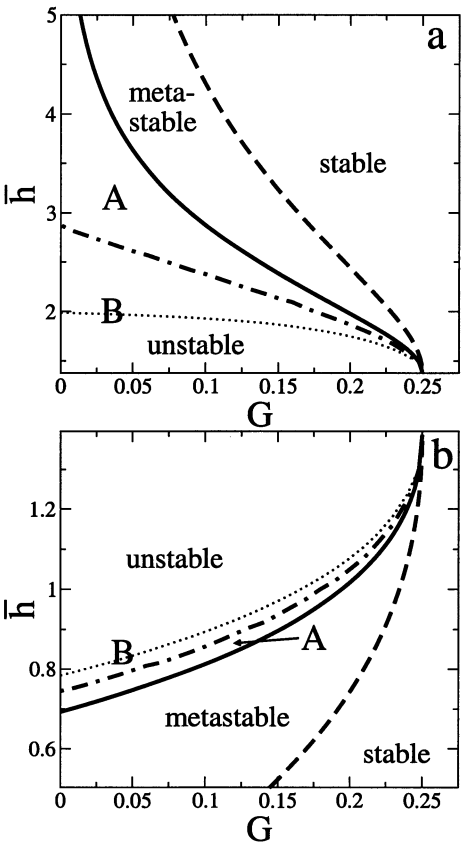

Fig. 8. The different rupture regimes for disjoining pressure (I) are shown within the plane (G, $\bar{h}$) for (a) $\bar{h} > h_c$ and (b) $\bar{h} < h_c$. The linearly unstable range lying to the left of the solid line is divided by the dot-dashed line in the nucleation-dominated subrange denoted A and the instability-dominated subrange denoted B. The dotted line shows the location where the branch of nucleation solutions ceases to exist, i.e. the border between (i) the instability range and (ii) the range of mixed behavior.

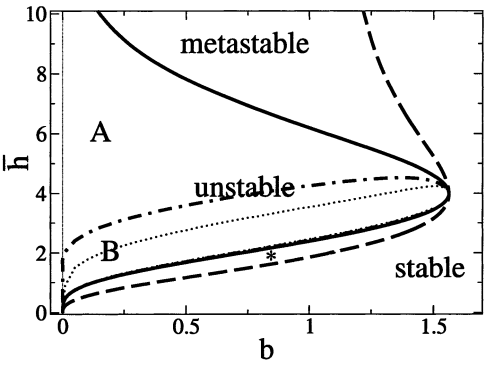

Fig. 9. The rupture regimes for disjoining pressure (II) are shown within the parameter plane (b, $\bar{h}$). Line styles and letters (A) and (B) are as in Fig. 8. The star denotes the lower metastable range.

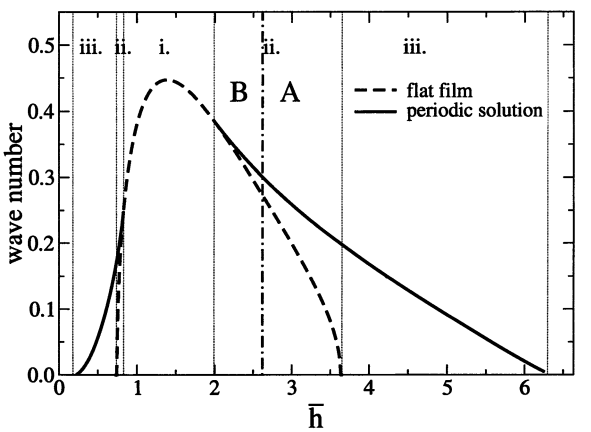

Fig. 10. Maximal wave number for nucleation solutions and linearly unstable mode for flat film according to the value of the mean film thickness. Shown are results for disjoining pressure (I) and $G = 0.05$. The dot-dashed vertical line indicates the value of $\bar{h}$ on the border between (A) and (B).

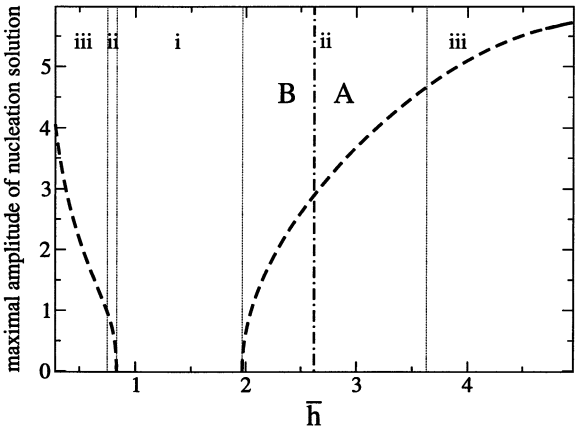

Fig. 11. Maximal amplitude of nucleation solution according to the value of the mean film thickness. Shown are results for disjoining pressure (I) and $G = 0.05$. The dot-dashed line is as in Fig. 10.

modes as $k = 2\pi/p$. Fig. 11 shows that the amplitude of the nucleation solution with the largest wave number goes to zero with power law behavior when the film thickness approaches the border between (i) and (ii). This allowed the unambiguous numerical identification of this border for the different disjoining pressures.

Beside the thin dotted lines, denoting the borders between (i), (ii) and (iii) the thick dot-dashed line shows the border between nucleation-dominated subrange (A) and instability-dominated subrange (B) as defined above. Especially, Fig. 11 shows that in subrange (B) close to the border between (A) and (B) even relatively large disturbances with amplitudes around 2.0 should not have a mayor influence on the time evolution. However, with respect to subrange (A), Fig. 11 only tells that there are large amplitude nucleation solutions that do influence the dynamics but does not allow to estimate a lower limit for their amplitude. For that purpose we show the dependence of growth rate on amplitude of some branches of nucleation solutions in Fig. 12. In the case shown, for $\bar{h} = 3.0$ the disturbance has to be deeper than approximately $\Delta h = 1$ to win over the fastest flat film mode (its growth rate is indicated by the horizontal line in Fig. 12), whereas for $\bar{h} = 3.5$ nearly all disturbances are faster than the flat film modes.

5. Disjoining pressure (III)

Both disjoining pressures dealt with up to now, combine a destabilizing short-range and a stabilizing long-range interaction (we regard the hydrostatic pressure in case (I) for a moment as part of the disjoining pressure). Therefore, the parameter planes Figs. 8 and 9 look very similar. Comparing Figs. 4–6 with the corresponding figures in [43] also confirms the similarity of the qualitative behavior of all the found solution families. However, we have still to show, that our main conclusions are also valid for quite different disjoining pressures like the ones that combine a stabilizing short-range and a destabilizing long-range interaction.

In this section we perform all the analysis steps introduced up to now, for the disjoining pressure denoted case (III) in Section 2.2. Using the results on the linear stability and metastability of the flat film we plot the parameter plane shown in Fig. 13. The solid line, that is identical to the solid line in Fig. 9 separates again linearly stable and linearly unstable thickness ranges. However, in contrast to the 'inverse' case (II), there exists no absolutely stable thickness range, all the linearly stable flat films can rupture if the finite disturbance is large enough.

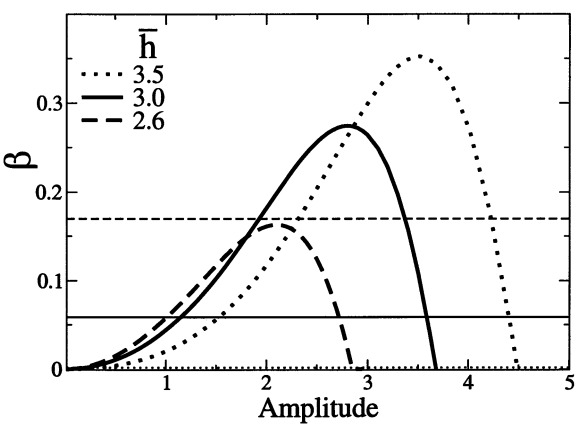

Fig. 12. Shown is the dependence of the growth rate of the fastest unstable eigenfunction on amplitude of the stationary solution for the nucleation solutions at $G = 0.05$ and mean film thicknesses as given in the legend. The thin horizontal lines give the respective growth rates of the fastest unstable flat film mode for the corresponding mean film thickness.

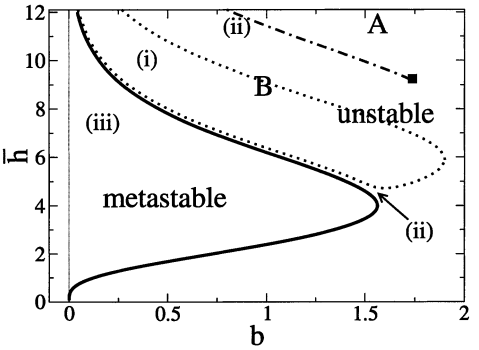

Fig. 13. The rupture regimes for disjoining pressure (III) are shown within the parameter plane (b, $\bar{h}$). A and B denote, respectively, the nucleation-dominated and instability-dominated subranges within the linearly unstable thickness range (to the right of the solid line). They are separated by the dot-dashed line. For a discussion of the terminating point of this line see main text. The dotted line is the border between (i) the instability range and (ii) the range of mixed behavior. The metastable range is to the left of the solid line. The thin vertical line marks the value $b = 0$. Take note, that ranges (i) and (ii) are only shown for $h > h_c = 4$. Similar ranges exist for $h < h_c$, but are not shown here.

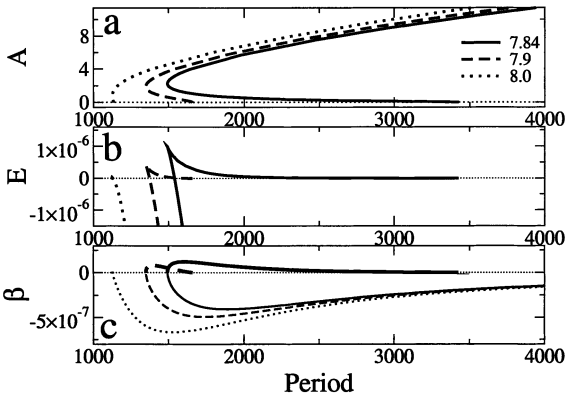

Fig. 14. Characterization of the solution families for disjoining pressure (III) at fixed $b = 0.5$. The mean film thicknesses, $\bar{h}$, for the respective curves is given in the legend. Shown are (a) the amplitude, (b) the energy and (c) the growth rate as a function of period. The energies are relative to the respective flat film energies. With increasing film thickness the family type changes from (ii) to (i).

Analyzing the families of stationary periodic solutions one finds again, the separation of the linearly unstable range into a subrange where no nucleation solutions exist and a subrange where these solutions exist. Denoted, respectively, by (i) and (ii), and the metastable range by (iii) as before, they are shown in Fig. 13. There is one range of mixed behavior (ii) extending towards infinite film thickness above the range (i) and another one between (i) and (iii), as indicated by the arrow. Take note, that the thickness ranges (i) and (ii) are only shown for thicknesses above the metastable range. Similar ranges do also exist below the metastable range.

Studying the dependencies of amplitude, energy and growth rate of perturbations on period for the families of periodic solutions for b smaller than one, it can be seen that the families are qualitatively similar as for disjoining pressures (I) and (II). This is illustrated in Fig. 14 for the transition between the regimes (ii) and (i) when increasing the film thickness directly above the metastable range and in Fig. 15 for the transition from (i) to (ii) occurring at larger film thicknesses. An important difference to cases (I) and (II) is the role of the large amplitude branches in Fig. 14(a) and Fig. 15(a). For (I) and (II) they are (when fixing the period) linearly and absolutely stable because they remain between the two thicknesses with lowest energy, g, (Eq. (26)). Here, however, $g \to -\infty$ for $h \to 0$. This implies that the large amplitude branch is only metastable and certain perturbations that overcome another nucleation solution will cause true film rupture in case (III). This second large-amplitude nucleation branch

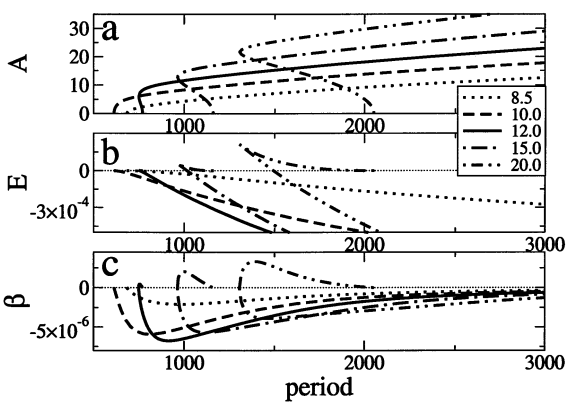

Fig. 15. Solution families for disjoining pressure (III) at fixed $b = 0.5$ for larger film thicknesses than in Fig. 14. Parts (a) to (c) and the legend are as in Fig. 14. With increasing film thickness the family type changes from (i) to (ii).

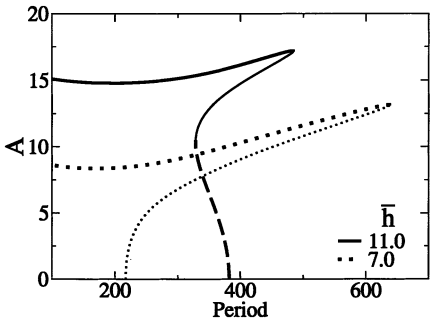

Fig. 16. The dependence of amplitude on period is shown for disjoining pressure (III) for $b = 1.4$. The curve for $\bar{h} = 7.0$ has two branches; the stable small amplitude branch is denoted by the thin dotted line and the unstable large amplitude branch by the thick dotted line. For $\bar{h} = 11.0$ three branches exist; beside the stable (thick solid line) and unstable (thick dotted line) as for $\bar{h} = 7.0$ a third, unstable small amplitude branch exits (dashed line).

can be seen directly for larger b. There the linearly stable branch does no continue towards infinite period but terminates at a saddle-node bifurcation at a certain period as can be seen in Fig. 16. This happens independently of the behavior for small amplitudes, i.e. in all regimes, (i), (ii) and (iii). The interpretation of the newly found branch as a second nucleation branch, i.e. as the threshold of true rupture is confirmed by the energy of the solutions (Fig. 17) and the growth rate, β, as calculated from the linear stability analysis of the solutions on the different branches (Fig. 18). Some solutions are shown in Fig. 19. The large

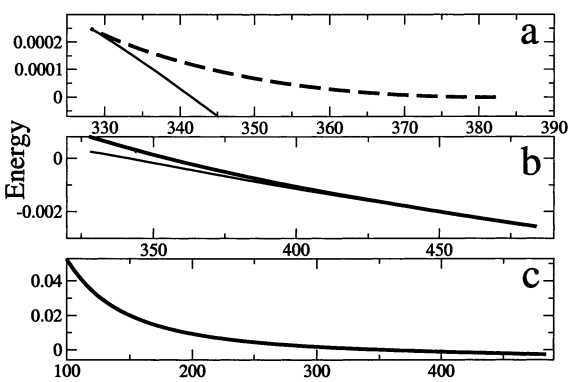

Fig. 17. The dependence of energy on period is shown for the $\bar{h} = 11.0$ curve from Fig. 16. Parts (a)–(c) show different period and energy ranges. Line styles are as in Fig. 16.

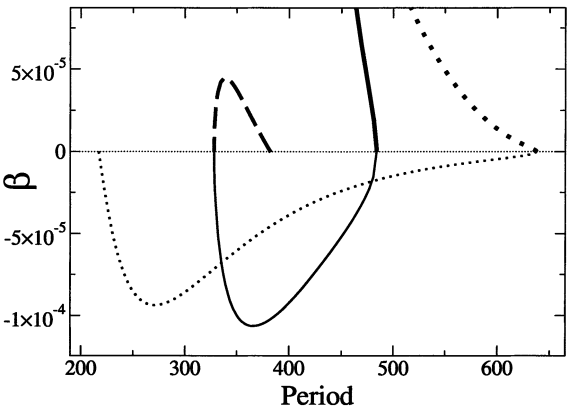

Fig. 18. The dependence of growth rate, β on period is shown for $\bar{h} = 11.0$ and $\bar{h} = 7.0$ for $\beta = 1.4$ Line styles are as in Fig. 16.

amplitude nucleation solution (dotted line) resembles closely the linearly stable solution (solid line). However, the local difference in the amplitude is not negligable.

As in cases (I) and (II) we would like to determine the thickness range where the small amplitude nucleation branch has an significant influence on the time evolution of a flat perturbed film. The border between the subranges (A) and (B) of the linearly unstable thickness range is defined as before. It is the film thickness where the

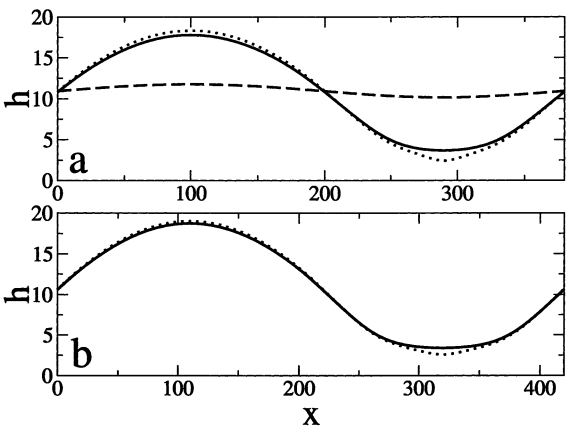

Fig. 19. Film thickness profiles for $\bar{h} = 11.0$ and $b = 1.4$ for (a) $L = 420$ and (b) $L = 380$. The solid lines are the respective linearly stable solutions, the dotted lines are the large amplitude unstable solutions and the dashed line in (a) is the small amplitude unstable solution.

maximal growth rates of a small disturbance are equal for the flat film and for the periodic nucleation solutions on the small amplitude branch. Since here, in contrast to cases (I) and (II), two nucleation branches exist, we have to introduce the latter restriction. The numerically calculated line separating the nucleation-dominated (A) and the instability-dominated (B) is plotted in Fig. 13. Note, that this line ends at $b \approx 1.7$. This is due to the fact, that at about this value of b the linearly stable solution branch ceases to exist, leaving only one nucleation branch and rendering the above definition obsolete.

Finally, we show the difference between (A) and (B) by directly integrating the time dependent Eq. (7) for a system of size $n\lambda_m$ taking as an initial condition a flat film with a localized disturbance

$$h_{\text{init}} = \bar{h}\left[1 - d\cosh\left(\frac{x}{w\lambda_m}\right)^{-2}\right] \tag{33}$$

with periodic boundary conditions. $n > 1$ is an integer, λ_m is the wavelength of the fastest growing flat film mode for $\bar{h}$, d is the maximum disturbance depth in units of $\bar{h}$, and w a measure of its width in terms of λ_m. Also in the case of disjoining pressure (III) the time evolutions for different initial disturbances and mean thicknesses permit the qualitative distinction of the two thickness regions, (A) and (B), within the linearly unstable thickness range as introduced for disjoining pressures (I) and (II) in Section 4 and indicated in Fig. 13.

5.1. Nucleation-dominated subrange (A)

The growth of the initial disturbance and eventual secondary nucleation events determine the evolution as shown with an example in Fig. 20(b). The final, short-time structure, observed before on a larger time scale coarse graining sets in, is a set of holes with distances, that are unrelated to the wavelength of the fastest flat film mode, λ_m (last curve of Fig. 20(b)). Details of the evolution and the resulting spatial structure depend strongly on the width and depth of the initial disturbance as can be seen in the Fourier spectra of a set of final structures (Fig. 21(b)) or in the evolution of the spatially averaged energy resulting in different

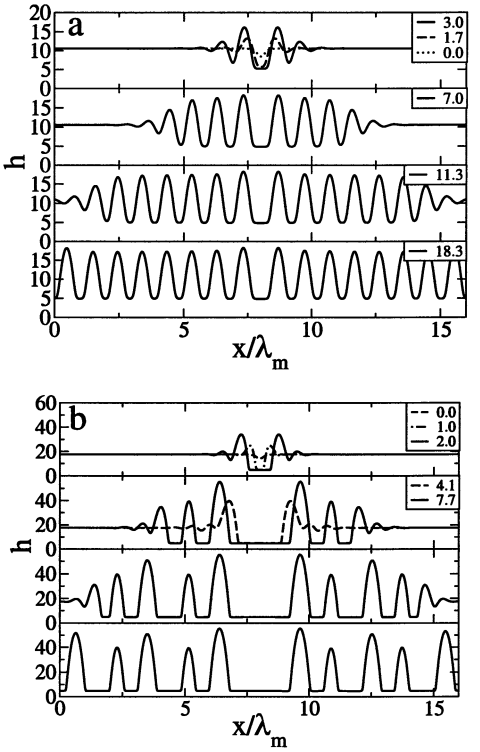

Fig. 20. Short-time evolution for a localized disturbance with $d = 0.2$ and $w = 0.2$ at $b = 1.0$ for disjoining pressure (III), (a) instability-dominated at $\bar{h} = 10.5$ and (b) nucleation-dominated at $\bar{h} = 17.5$. The coordinate x is shown in units of the wavelength corresponding to the fastest growing linear mode, λ_m. In-sets give the time in units of the growth time, $\tau_m = 1/\beta_m$, of the same mode.

values for the final short-time structure (shown in Fig. 22(b)). In the change of the energy with time one can clearly see the individual secondary nucleation events, that give the process a step-like character.

5.2. Instability-dominated subrange (B)

The initial disturbance induces the sideward and downward growth of undulations having from the beginning the wavelength of the most unstable flat film mode that eventually determines the final short-time structure as shown in Fig. 20(a). This final structure is a nearly periodic set of holes whatever the width and depth of the initial perturbation used, as shown in the Fourier

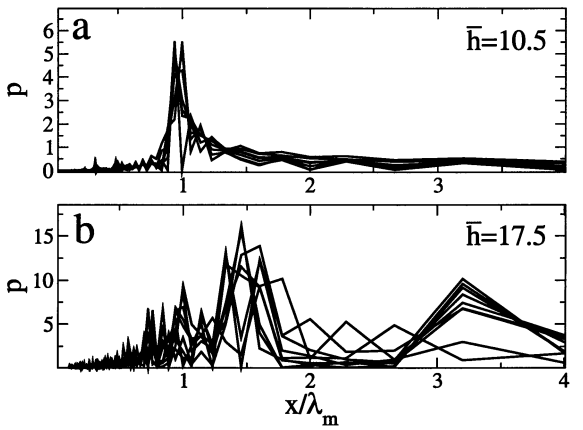

Fig. 21. Fourier transforms of the final short-time, spatial patterns for at time $t/\tau_m = 17$ (a) $\bar{h} = 10.5$ and (b) $\bar{h} = 17.5$. Both figures show results for a number of runs for different depth′ ($d = 0.1$–0.4) and width′ ($w = 0.1$–0.4) of the initial disturbance for $b = 1.0$. x-axis as in Fig. 20.

spectra of a set of final structures in Fig. 21(a). The evolution of the energy (Fig. 22(a)) depends only in its early stage on the size of the initial disturbance. Then it decreases approximately linear showing that the lateral extension of the instability is a smooth process of constant velocity. In contrast to (A) different initial disturbances result in the same energy for the final short-time structure corresponding to the energy of the stationary solution of period, P, equal to the wavelength of the fastest flat film mode, λ_m. The qualitative features of the transition between (A) and (B) are the same as for disjoining pressures (I) and (II), discussed already in Section 4. However, the range where one finds mixed structures seems to be larger than in the other cases. To clearly illustrate the transition we choose, therefore, to show the time evolution for $\bar{h} = 10.5$ and $\bar{h} = 17.5$ at $b = 1.0$.

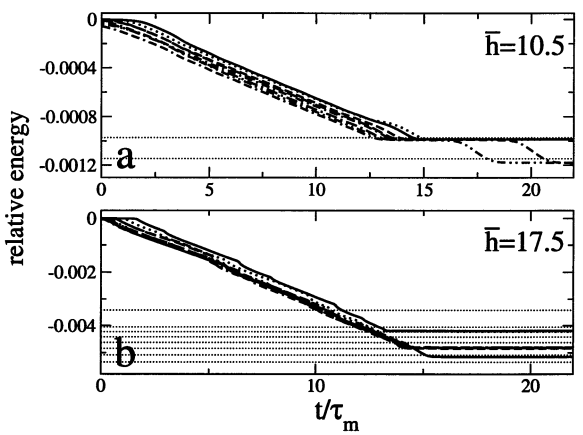

Fig. 22. Average energies subtracted that of the corresponding flat film are plotted for the short-time evolution at (a) $\bar{h} = 10.5$ and (b) $\bar{h} = 17.5$. A number of runs is shown as in Fig. 21 (thick lines, different line styles). The thin horizontal lines represent the energy for stationary solutions with the following respective periods (from above): (a) $P = \lambda_m$, $P = 16\lambda_m/15$ and (b) $P = \lambda_m$, $16\lambda_m/12$, $16\lambda_m/11$, $16\lambda_m/10$, $16\lambda_m/9$, $16\lambda_m/8$, $16\lambda_m/7$, $16\lambda_m/6$. Note that in (a) two of the curves show the first coarsening events (downward steps at about $t/\tau_m = 18$) that determine eventually the long-time evolution towards a single remaining drop.

6. Discussion and conclusion

We have analyzed the evolution of a thin liquid film under the influence of three different disjoining pressures: (I) a disjoining pressure arising in diffuse interface theory [38], (II) a combination of a destabilizing short-range polar and a stabilizing long-range apolar interaction, and (III) the inverse of case (II), a combination of a stabilizing short-range polar and a destabilizing long-range apolar interaction.

After discussing the stable, metastable and linearly unstable thickness ranges according to the values of the respective control parameters and studying the existing flat film solutions, we have discussed the families of stationary periodic and localized solutions and their linear stability. In the metastable film thickness ranges we have identified periodic and localized nucleation solutions that separate decaying and growing finite disturbances. Furthermore, a second branch of periodic solutions was found consisting of solutions that are linearly stable taking their period as unit for the stability analysis. However, as shown in [43] they are unstable to coarsening. The results regarding the families of periodic nucleation solutions, can be used to extend the findings of single critical droplets and holes for first-order wetting transitions [50,51] towards finite periods. For all the disjoining pressures studied, in the

linearly unstable film thickness range we have distinguished two subranges with different prevailing rupture mechanisms: (A) nucleation-dominated and (B) instability-dominated regions. In the nucleation-dominated subrange small-scale initial finite disturbances determine the final structure whereas the unstable flat film modes are too slow to influence the structure formation. In the instability-dominated subrange the evolution is controlled by the fastest flat film mode and finite disturbances have only negligible influence. This was confirmed by direct integration of the time evolution Eq. (7) for case (I) in [43], for case (II) in [42] and for case (III) in Section 5. Despite the restriction to a two-dimensional geometry we think that the difference of subranges (A) and (B) can also be seen in the more realistic three-dimensional geometry.

The results obtained here for the two most important cases of disjoining pressures with antagonistic long- and short-range influences, namely, short-range stabilizing combined with long-range destabilizing influences and vice versa coincide in their main conclusions. This leads us to the assumption that the distinction of subranges (A) and (B) is also valid for other disjoining pressures consisting of two or more components.

The results on the families of stationary solutions are especially apt to be compared with existing numerical integrations of film evolution equations. It is very convenient to determine the parameter ranges where true film rupture can occur (in case (III)) and where not. The small difference between the linearly stable profile and the large-amplitude nucleation solution that lies between this profile and film rupture shows that it is easily possible to miss the stable profile in a numerical simulation of the time evolution choosing the timestep to large.

Furthermore we would like to point out, that the results for disjoining pressures (II) and (III) especially complement [33] where they studied the time evolution of a flat film with initial finite amplitude sinusoidal perturbations. However, they choose wavelength that are larger than the critical wavelength for the flat film, λ_c, and calculate the nonlinear time evolution to get a correction of the predictions for film rupture from linear theory. In contrast, the analysis of the nucleation solutions in the linearly unstable film thickness range that is performed here focuses on small scale disturbances (defects) with lateral extensions smaller than λ_c. Also, we do not calculate non-linear corrections of linear predictions for rupture but compare linear growth rates of perturbations to the flat film and to the nucleation solutions.

Beside the qualitatively similar main result for the different disjoining pressures, namely the existence of the subranges (A) and (B), important details differ as can best be seen by comparing the position and extension of stable, metastable and linearly unstable thickness ranges in the parameter planes Figs. 8 and 9 and Fig. 13. The comparison of cases (I) and (II) can already be found in [43] and Section 5 explained the main differences of case (III) when compared with (I) and (II). Especially the divergence of the disjoining pressure for vanishing film thickness in cases (II) and (III) has a mayor influence on the behavior at small b, that differs strongly from the behavior for small G in case (I).

Nucleation in the linearly unstable thickness range was also investigated in systems that undergo spinodal decomposition. To compare our results with these systems the film thickness used here has to be replaced by the concentration of one component. Close to the critical point in the parameter plane (G_c or b_c, h_c) the derivative of the free energy in the evolution equation for the film thickness Eq. (7) can be approximated by a quartic polynomial and Eq. (7) reduces to the Cahn–Hilliard equation (Appendix of [43]). Some aspects discussed here for different disjoining pressures were described for different variants of the Cahn–Hilliard equation. A study of the stationary periodic concentration profiles led to a qualitative distinction corresponding to our regimes (i), (ii), and (iii) [45]. However, in that work they did not determine the boundary between the pure instability regime (i) and the regime of mixed behavior (ii). They already identified the positive-energy branch within the metastable range (iii) as periodic nucleation-type solutions [45] and suggested that 'the phase separation in the deep spinodal region, may be distin-

guishable, perhaps more nearly periodic or 'spinodal', than in the rest of the spinodal region' [46]. The latter hypothesis we confirm with our distinction between (A) nucleation-dominated and (B) instability-dominated subranges within the linearly unstable thickness range. [47] studied the short-time behavior of multilayer systems with the one-dimensional Cahn–Hilliard equation. Using an energy analysis, they focused on the relative stability of periodic concentration profiles and constant concentration solutions when fixing the period, as a result they establish concentration ranges for absolute stability, metastability and linear instability of the different solutions. Their discussion corresponds to part of our discussion of the different solution families, especially in the regimes (ii) and (iii). These analogies point out that our findings are also relevant for the explication of phenomena occurring in spinodal decomposition. In particular, the conjecture formulated in [46] that the system behavior in a subrange of the spinodal concentration range is highly disturbance-dependent can be made more precise using the quantitative description reviewed and extended here.

Acknowledgements

This research was supported by the European Union under ICOPAC grant HPRN-CT-2000-00136, by the German Academic Exchange Board (DAAD) under grant D/98/14745, by the Deutsche Forschungsgemeinschaft (DFG) under grant TH781/1 and by the Spanish Ministry of Science and Technology under grant PB 96-599. We thank M. Bär, U. Bahr, M. Bestehorn, L. Brusch, G. Diener, K. Jacobs, M. Mertig, A. Oron, L. Pismen, G. Reiter, A. Sharma, R. Seemann, V. Starov for helpful discussions and comments.

References

[1] A. Oron, S.H. Davis, S.G. Bankoff, Rev. Mod. Phys. 69 (1997) 931.
[2] H.S. Kheshgi, L.E. Scriven, Chem. Eng. Sci. 46 (1991) 519.
[3] M. Mertig, U. Thiele, J. Bradt, D. Klemm, W. Pompe, Appl. Phys. A66 (1998) S565.
[4] F. Brochard-Wyart, J. Daillant, Can. J. Phys. 68 (1989) 1084.
[5] G. Reiter, Phys. Rev. Lett. 68 (1992) 75.
[6] E. Ruckenstein, R. Jain, J. Chem. Soc. Faraday Trans. 1170 (1974) 132.
[7] R. Khanna, A. Sharma, G. Reiter, EPJdirect E2 (2000) 1.
[8] R. Seemann, K. Jacobs, S. Herminghaus, Phys. Rev. Lett. 86 (2001) 5534.
[9] C. Redon, F. Brochard-Wyart, F. Rondelez, Phys. Rev. Lett. 66 (1991) 715.
[10] K. Jacobs, R. Seemann, G. Schatz, S. Herminghaus, Langmuir 14 (1998) 4961.
[11] G. Reiter, R. Khanna, Phys. Rev. Lett. 85 (2000) 2753.
[12] K. Jacobs, S. Herminghaus, K.R. Mecke, Langmuir 14 (1998) 965.
[13] G. Reiter, A. Sharma, A. Casoli, M.-O. David, R. Khanna, P. Auroy, Langmuir 15 (1999) 2551.
[14] G. Reiter, R. Khanna, A. Sharma, Phys. Rev. Lett. 85 (2000) 1432.
[15] V. Mitlin, J. Colloid Interf. Sci. 233 (2001) 153.
[16] A. Sharma, G. Reiter, J. Colloid Interf. Sci. 178 (1996) 383.
[17] K. Jacobs, Stabilität und Dynamik flüssiger Polymerfilme, (1997), Ph.D.-thesis, ISBN 3-930803-10-0.
[18] N. Samid-Merzel, S. Lipson, D.S. Tannhauser, Phys. Rev. E57 (1998) 2906.
[19] J. Bischof, D. Scherer, S. Herminghaus, P. Leiderer, Phys. Rev. Lett. 77 (1996) 1536.
[20] R. Xie, A. Kartim, J. Douglas, C. Han, R. Weiss, Phys. Rev. Lett. 81 (1998) 1251.
[21] U. Thiele, M. Mertig, W. Pompe, Phys. Rev. Lett. 80 (1998) 2869.
[22] G. Reiter, Langmuir 9 (1993) 1344.
[23] J.W. Cahn, J.W. Hillard, J. Chem. Phys. 28 (1958) 258.
[24] V.S. Mitlin, J. Colloid Interf. Sci. 156 (1993) 491.
[25] B.V. Derjaguin, Zh. Fiz. Khim. 14 (1940) 137.
[26] B.V. Derjaguin, N.V. Churaev, V.M. Muller, Surface Forces, Consultants Bureau, New York, 1987.
[27] G.F. Teletzke, H.T. Davis, L.E. Scriven, Rev. Phys. Appl. 23 (1988) 989.
[28] R.J. Hunter, Foundation of Colloid Science, vol. 1, Clarendon Press, Oxford, 1992.
[29] J.N. Israelachvili, Intermodular and Surface Forces, Academic Press, London, 1992.
[30] V.M. Starov, Adv. Colloid Interf. Sci. 39 (1992) 147.
[31] A. Sharma, Langmuir 9 (1993) 861.
[32] A. Sharma, J. Colloid Interf. Sci. 156 (1993) 96.
[33] A. Sharma, A.T. Jameel, J. Colloid Interf. Sci. 161 (1993) 190.
[34] A.T. Jammel, A. Sharma, J. Colloid Interf. Sci. 164 (1994) 416.
[35] A. Sharma, R. Khanna, Phys. Rev. Lett. 81 (1998) 3463.

[36] A. Sharma, R. Khanna, J. Chem. Phys. 110 (1999) 4929.
[37] A. Oron, Phys. Rev. Lett. 85 (2000) 2108.
[38] L.M. Pismen, Y. Pomeau, Phys. Rev. E62 (2000) 2480.
[39] A. Sharma, Langmuir 9 (1993) 3580.
[40] P. de Gennes, Rev. Mod. Phys. 57 (1985) 827.
[41] U. Thiele, K. Neuffer, M. Bestehorn, Y. Pomeau, M.G. Velarde, Colloids Surf. A: Physicochem. Eng. Aspects, 206 (2002) 87–104.
[42] U. Thiele, M.G. Velarde, K. Neuffer, Phys. Rev. Lett. 87 (2001) 016104.
[43] U. Thiele, M.G. Velarde, K. Neuffer, Y. Pomeau, Phys. Rev. E64 (2001) 031602.
[44] J. Langer, Ann. Phys. 65 (1971) 53.
[45] A. Novick-Cohen, L.A. Segel, Physica D 10 (1984) 277.
[46] A. Novick-Cohen, J. Stat. Phys. 38 (1985) 707.
[47] M. Hentschel, M. Bobeth, G. Diener, W. Pompe, Thin Solid Films 354 (1999) 267.
[48] A. Oron, P. Rosenau, J. Phys. (France) II 2 (1992) 361.
[49] V. Mitlin, J. Colloid Interf. Sci. 227 (2000) 371.
[50] R. Bausch, R. Blossey, Phys.Rev. E48 (1993) 1131.
[51] R. Bausch, R. Blossey, M. Burschka, J. Phys. A27 (1994) 1405.
[52] E. Doedel, A. Champneys, T. Fairfrieve, Y. Kuznetsov, B. Sandstede, X. Wang, AUTO97: Continuation and Bifurcation Software for Ordinary Differential Equations, Concordia University, Montreal, 1997.